THE JOURNAL OF PHYSICAL CHEMISTRY B
A JOURNAL OF THE AMERICAN CHEMICAL SOCIETY

pubs.acs.org/JPCB

Article

Thermodynamic Driving Forces of Redox-Dependent CPR Insertion into Biomimetic Endoplasmic Reticulum Membranes

Michael J. Martinez, Jessica D. Carder, Evan L. Taylor, Eric P. Jacobo, ChulHee Kang, and J. A. Brozik*

Cite This: *J. Phys. Chem. B* 2022, 126, 1691−1699

Read Online

ACCESS | Metrics & More | Article Recommendations | Supporting Information

ABSTRACT: Cytochrome P450 reductase (CPR) is a NADPH-dependent membrane-bound oxidoreductase found in the endoplasmic reticulum (ER) and is the main redox partner for most cytochrome P450 enzymes. Presented are the measured thermodynamic driving forces responsible for how strongly CPR partitions into a biomimetic ER with the same lipid composition of a natural ER. Using temperature-dependent fluorescence correlation spectroscopy and fluorescence single-protein tracking, the standard state free energies, enthalpies, and entropies of the CPR insertion process were all measured. The results of this study demonstrate that the thermodynamic driving forces are dependent on the redox states of CPR. In particular, the partitioning of CPR^{ox} into a biomimetic ER is an exothermic process with a small positive change in entropy, while CPR^{red} partitioning is endothermic with a large positive change in entropy. Both resulted in negative free energies and strong association to the biomimetic ER, but the K_P of CPR^{ox} insertion is measurably smaller than that of CPR^{red}. Using this new information and known results from literature sources, we also present a phenomenological model that accounts for membrane−protein interactions, protein orientation relative to the membrane, and protein conformation as a function of the redox state.

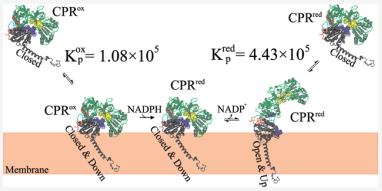

1. INTRODUCTION

Cytochrome P450 reductase (CPR) is found on the cytoplasmic side of the ER membrane and is the main redox partner for most cytochrome P450 enzymes. The electrons supplied by CPR (though oxidation of NADPH) allow P450 enzymes to perform oxidative transformations on many drugs, small molecules, and important biomolecules.[1−3] CPR is composed of four distinct domains: (i) a NADPH/FAD domain, (ii) an FMN domain, (ii) a hinge domain, and (iv) a membrane binding domain. The NADPH/FAD domain contains a NADPH binding pocket and a flavin adenosine dinucleotide (FAD).[4] Likewise, the FMN domain contains a flavin mononucleotide (FMN).[5] The NADPH/FAD and FMN domains are connected to one another through the flexible hinge domain allowing CPR to exist in an equilibrium between a closed conformation in which the flavins (FAD and FMN) are in close contact and an open configuration in which the flavins are further away from one another. When CPR is in its oxidized form (CPR^{ox}), the equilibrium is shifted to the closed conformation.[6−9] When NADPH binds to CPR^{ox}, it transfers two electrons through a hydride ion transfer followed by interflavin electron transfer.[10] The open conformation of CPR is also required for delivery of electrons from the reduced FMN cofactor to the partner P450. When $NADP^+$ is released, the equilibrium of reduced CPR (CPR^{red}) shifts toward the open configuration.[1,7,11,12] It is in this open conformation that CPR is ready to transfer electrons to P450s to continue the catalytic cycle.[13]

We have previously reported that the redox state of CPR greatly affects how it interacts with and diffuses through a biomimetic ER membrane.[14] In that previous study, we used single-molecule techniques to demonstrate that CPR^{ox} has peripheral membrane characteristics while the direct observations made on CPR^{red} were most consistent with its designation as an integral membrane protein. In this regard, we directly observed CPR^{ox} entering a biomimetic ER membrane from solution and presented evidence for it leaving the biomimetic ER membrane at equilibrium. It was also shown that CPR^{red} has greater membrane incorporation and no evidence of CPR^{red} entering the ER membrane from solution. Moreover, we observed that CPR^{red} has a much slower diffusion coefficient than CPR^{ox} (1.5 $\mu m^2/s$ compared to 2.5 $\mu m^2/s$), indicating that CPR^{red} is more deeply embedded into to the ER membrane than CPR^{ox}.

In this work, we have used temperature-dependent fluorescence correlation spectroscopy (FCS) and fluorescence single-protein tracking in a mimetic of the ER to quantitatively measure the concentration of CPR in the membrane and in solution as a function of the redox state and temperature. (Note: the "biomimetic ER membrane" is referred to as "ER" throughout the rest of the manuscript.) This approach has allowed for the determination of thermodynamic driving forces

Received: October 28, 2021
Revised: February 2, 2022
Published: February 16, 2022

(ΔG^{o}, ΔH^{o}, and ΔS^{o}) for CPR partitioning from solution into the ER. This study has revealed fundamentally different driving forces for the oxidized and reduced forms of CPR and how it interacts with the membrane. This information was used in conjunction with recent theoretical and earlier solution phase studies to develop a phenomenological model that accounts for membrane−protein interactions, protein orientation relative to the plane of the membrane, and protein conformation as a function of the redox state.[7,9,12,15]

2. METHODS

2.1. Materials. D-Glucose, catalase, and glucose oxidase were purchased from Sigma-Aldrich (St. Louis, MO). NADPH was purchased from EMD Millipore (Billerica, MA). All lipids were purchased from Avanti Polar Lipids (Alabaster, AL).

2.2. Protein Expression, Purification, and Labeling. Full-length human CPR was expressed, purified, and stored as previously reported.[16] After purification, CPR was labeled with Alexa 680 C_2 Maleimide (Thermo Fisher Scientific, Waltham, MA). Briefly, Alexa 680 C_2 Maleimide was dissolved in 100% HPLC grade acetonitrile, stored at −20 °C in the dark, and used in the following 24 h. CPR was diluted to 15 μM in 100 mM HEPES (pH 7.4) buffer containing 150 mM NaCl and 20% glycerol (v/v). The solution was transferred to a sealed glass vial and gently degassed for 5 min under Ar while kept on ice. The dye was added to the degassed protein containing solution in a 1:1.2 protein:dye concentration ratio and allowed to react under gentle stirring at 4 ° C overnight while protecting the reaction mixture from light. The reaction was stopped by addition of a 1 M solution of DTT to a final concentration of 3 mM. The labeled CPR was then purified from the excess dye by using a desalting Micro Bio-Spin column packed with Bio-Gel P-6 (BioRad, Hercules, CA). The gel in the column was suspended in Tris buffer (pH 7.4) but was exchanged with 100 mM HEPES (pH 7.4) containing 140 mM NaCl and 5 mM $CaCl_2$ (referred to as ER buffer). The degree of labeling was calculated according to the protocol and estimated to be 1. The labeled CPR was then aliquoted, flash frozen in liquid N_2, and stored at −80 °C.

2.3. Preparation of Small Unilamellar Vesicles. A phospholipid mixture matching the chemical composition of the human ER membrane has been developed and described by our laboratory.[14,17] To this mixture, a polyethylene glycol (PEG) cushion was also incorporated into the membrane to prevent unwanted interactions between CPR and the underlying glass substrate when formed into a supported lipid bilayer (see below). In this study, small unilamellar vesicles (SUVs) were made from 1.42 μmol of 1,2-dilauroyl-*sn*-glycero-3-phosphocholine (DLPC), 1.42 μmol of 1,2-dioleoyl-*sn*-glycero-3-phosphocholine (DOPC), 1.0 μmol of 1-palmitoyl-2-oleoyl-*sn*-glycero-3-phosphoethanolamine (POPE), 0.35 μmol of 1,2-dilauroyl-*sn*-glycero-3-phospho-L-serine (sodium salt) (DLPS), 0.20 μmol of cholesterol, 0.35 μmol of l-α-phosphatidylinositol-4,5-bisphosphate, 0.19 μmol of sphingomyelin, and 0.07 μmol of 1,2-dioleoyl-*sn*-glycero-3-phosphoethanolamine-*N*-[methoxy(polyethylene glycol)-2000] (ammonium salt) (PEG−PE). The mixture was dissolved in 1 mL of chloroform and placed in a 5 mL round bottom flask. The flask was then placed under a flow of pre-purified nitrogen to evaporate the chloroform to form a cake. Next, large multilamellar vesicles (LMVs) were formed by hydrating the lipid cake with 1 mL of ER buffer (100 mM HEPES, 5 mM $CaCl_2$, and 140 mM NaCl at pH 7.4). The mixture was then placed in a water bath at 60 °C, gently swirled every 15 min for 1 h, and then sonicated in a bath sonicator at 60 °C for 30 min to form the SUVs. During this time, the solution turned from turbid to transparent. Next, the solution was place in a centrifuge for 2 h at 13,000*g* and 37 °C. The supernatant was then removed, aliquoted, flash frozen in liquid N_2, and stored at −80 °C.

2.4. Formation of Planar-Supported Lipid Bilayers. Planar-supported lipid bilayers were prepared according to a protocol described earlier.[14,17−19] Briefly, 25 mm round quartz coverslips were gently boiled in a solution of water, concentrated nitric acid, and 30% hydrogen peroxide (1:1:1 by volume) while gently swirling to separate the cover glass for 15 min. The coverslips were then rinsed thoroughly with water that was purified by a Barnstead Nanopure 18 MΩ organic free water purifier (referred to as nanopure water). This treatment was performed twice, and then, the coverslips were stored under nanopure water with daily retreatment before use. Before lipid bilayer formation, a coverslip was removed from the storage container, rinsed with a stream of nanopure water, and then dried under a stream of pre-purified nitrogen. The coverslip was then placed in a custom-built sample holder and affixed with a 6 mm inner radius paraffin gasket that was sealed to the coverslip with the gentle application of heat. Next 50 μL of the solution containing the SUVs was added to the center of the coverslip and allowed to incubate for 1 h at room temperature. During this time, the SUVs fused to the hydrophilic surface of the coverslip, ruptured, and formed a continuous supported lipid bilayer. Finally, the newly formed supported lipid bilayer was rinsed six times with the ER buffer to remove any excess SUVs. This planar-supported bilayer is referred to as an ER membrane in the rest of the article. This ER membrane has previously been characterized via fluorescence recovery after photobleaching and shown to be homogeneous and one phase from 17 to 41 °C.

2.5. Preparation of Reduced and Oxidized CPR Samples. The insertion was done using previously published methods.[14,17,20] The resting state of CPR is its oxidized form. CPR^{ox} samples were prepared by first removing (by pipette) the ER buffer above the bilayer and replacing it with 25 μL of a 2.5 nM solution of CPR in an imaging buffer containing 0.8% w/v D-glucose, 1 mg/mL glucose oxidase, and 0.04 mg/mL catalase in ER buffer. The sample was immediately transferred to either the FCS microscope or the protein tracking microscope (see below) and allowed to reach equilibrium at the temperature of the experiment. Reduced CRP samples were prepared in the same manner as CPR^{ox} samples except that 2.5 nM NADPH was added to the imaging buffer. Measurements were made immediately after sample equilibrium. All experiments were carried out under anaerobic conditions by using the glucose oxidase/catalase oxygen scavenging system and sealing the sample from air.[12,20] According to Roberts et al., under anaerobic conditions, the addition of stoichiometric amounts of NADPH will leave CPR^{red} in the minus $2e^-$ state (CPR^{2-}). Excess amounts of NADPH will lead to the fully reduced $4e^-$ state (CPR^{4-}), but this state is known to be thermodynamically unstable and rapidly oxidizes in the presence of oxygen; therefore, CPR^{2-} is normally considered as the state leading to electron transfer in P450s and the one of interest in this study.[21−23]

2.6. Fluorescence Correlation Spectroscopy. All FCS measurements were performed on a homebuilt fluorescence confocal microscope. For excitation, a 635 nm (PicoQuant GmbH, Berlin, Germany) diode laser was used in cw mode.

https://doi.org/10.1021/acs.jpcb.1c09358
J. Phys. Chem. B 2022, 126, 1691−1699

The laser emission was coupled into a single-mode optical fiber (ThorLabs, Newton, New Jersey) with a zoom-fiber collimator (ThorLabs, Newton, New Jersey) to change the elliptical shape of the beam to a Gaussian beam shape. The laser was then recollimated and launched into free space using another zoom-fiber collimator and directed to the microscope optics by a series of broadband dielectric mirrors and finally passed through a laser line filter (635 nm, ThorLabs, Newton, New Jersey). The laser light was then reflected by a 640 nm dichroic mirror (FF640-FDi02, Semrock, Rochester, New York) and focused by a 60× 1.2 NA water-immersion microscope objective (UPLSAPO60XW, Olympus, Tokyo, Japan). The emitted fluorescence was then collected by the same objective, passed through the dichroic mirror and reflected by a broadband dielectric mirror (ThorLabs, Newton, New Jersey). The reflected light was focused by a tube lens (ThorLabs, Newton, New Jersey) onto a 50 μm pinhole to set the confocal geometry. The light that passed through the pinhole was then collimated using a lens and either passed or reflected by a 50:50 non-polarizing beam splitter (ThorLabs, Newton, New Jersey) and focused onto two separate single-photon counting modules (SPCMs) (SPCM-AQRH-14-FC Excelitas, Quebec, Canada). The output of the SPCMs was connected to a four-channel router (PHR 800, Picoquant GmbH, Berlin, Germany), and the output from the router was connected to a time-correlated single-photon counting system (PicoHarp 300, PicoQuant GmbH, Berlin, Germany). The microscope was equipped with temperature control at the sample and the objective with a custom-made sample holder and objective collar. Both were fitted with Peltiers (TEC3-2.5; ThorLabs, Newton, New Jersey) and interfaced to separate Meerstetter Engineering temperature controllers (model TEC-1091). The temperature was monitored at the sample with a Pt temperature sensor (TH100PT; ThorLabs, Newton, New Jersey) and the hot side of the Peltiers with a thermistor (TH10K; ThorLabs, Newton, New Jersey).

All data were collected, and FCS curves were generated in SymPhoTime 64 (Picoquant GmbH, Berlin, Germany). The confocal volume was determined to be 1.18 fL using a dilution method.[24] For the samples described in Section 2.5, each was placed on the microscope and allowed to equilibrate at the desired temperature (21, 25, 29, 33, and 37 °C) for 30 min on the microscope before data collection. The laser power was set to 100 μW before being reflected by the dichroic mirror and focused 30 μm above the coverglass. A fluorescence time trace was recorded for 10 min, and following the conclusion of the time trace, a new sample was placed on the microscope, which was allowed to incubate for 30 min and a 10 min time trace was recorded; this was repeated for a total of three fluorescence time traces at each temperature point. The experiment was repeated at all temperature points for both CPR^{red} samples and CPR^{ox} samples in triplicate. All analyses were also performed in Igor Pro 8 (Wavemetrics, Inc.).

2.7. Single-Protein Counting in Planar-Supported Lipid Bilayers. The instrument used for tracking CPR^{ox} and CPR^{red} in ER membranes has been described in detail previously.[14,17] Briefly, fluorescent samples were excited with a stabilized CW-He:Ne laser producing a 633 nm beam with the power adjusted to 0.8 mW at the sample using a neutral density filter wheel. The beam was first passed through a laser line filter (633/10×; Chroma Tech.) and then a 1/4 waveplate (WPQ05M-633; Thorlabs, Inc.) to produce a circular polarized laser beam. The beam was then directed by a series of mirrors and focused by a 200 mm lens onto the back edged of a 100× 1.45 N/A apochromatic TIRF microscope objective (Olympus Inc.) with a dichroic mirror (FF545/650-Di01; Semrock, Inc.). The beam was positioned along the far edge of the microscope object using a translation stage so that the angle of the excitation beam was greater than the critical angle between the glass water interface of the sample. This produced an evanescent field (through objective total internal reflection fluorescence microscopy; TIRF). This allows for the excitation of only a small area above the lipid bilayer and eliminates most of the fluorescence from the solution phase.

The emission from single fluorescently labeled proteins was then collected by the microscope objective, passed through the dichroic mirror, passed through a long-pass filter (ET655lp; Chroma Technologies Corp.), and imaged onto an EMCCD camera (iXon 888; Andor Tech.) with a 300 mm achromatic lens. The exposure time was set to 50 ms, and the frame rate was only slightly higher at 50.02 ms. Temperature control was maintained at the sample and the microscope objective with a custom-made sample holder and objective collar. Both were fitted with Peltiers (TEC3-2.5; Thorlabs Inc.) and interfaced to separate Meerstetter Engineering temperature controllers (model TEC-1091). The temperature was monitored at the sample with a Pt temperature sensor (TH100PT; Thorlabs Inc.) and the hot side of the Peltiers with a thermistor (TH10K; Thorlabs Inc.).

Sample preparation was identical to those described for the FCS experiments. Each temperature point (21, 25, 29, 33, and 37 °C) was collected in triplicate for CPR^{ox} and CPR^{red}. All samples were equilibrated at temperature for a minimum of 30 min before data collection. A minimum of 50 images was collected at different locations on each sample, giving a particle count greater than or equal to 1003 (see histograms in the Supporting Information). Counting was performed with a custom MATLAB (The Mathworks Inc.) script based on the work of Crocker and Grier, which has been implemented previously by our group.[14,17,25] In this analysis, only diffraction-limited particles with an intensity threshold set to 2.6 times the background were counted. Analysis was performed in MATLAB using custom scripts.

3. RESULTS

3.1. Temperature-Dependent Concentration Changes above ER Membranes. FCS is a sensitive method for measuring the concentration of fluorescent molecules (and fluorescently labeled proteins) in dilute solutions. Depicted in Figure 1 are FCS curves and fits for ATTO 680-labeled CPR^{ox} and CPR^{red} in the solution above the ER membrane at 21 and 37 °C. Five curves at 21, 25, 29, 33, and 37 °C were collected for each redox state of CPR. In all, 30 independent samples were prepared: 3 independent samples for each temperature point for both CPR^{ox} and CPR^{red}. The fits of the raw data are depicted in Figure S2 (see the Supporting Information) and using the model function for a singly labeled protein that is freely diffusing in solution is given in eq 1 below[26]

$$G(\tau) = \frac{1}{\langle C\rangle \cdot V_{\mathrm{eff}} \cdot N_{\mathrm{A}}} \cdot [1 - T_{\mathrm{eq}} + T_{\mathrm{eq}} \mathrm{e}^{-\tau/\tau_{\mathrm{T}}}] \cdot \left(1 + \frac{\tau}{\tau_{\mathrm{D}}}\right)^{-1} \left(1 + \left(\frac{s}{u}\right)^2 \frac{\tau}{\tau_{\mathrm{D}}}\right)^{-1/2} \quad (1)$$

https://doi.org/10.1021/acs.jpcb.1c09358
J. Phys. Chem. B 2022, 126, 1691−1699

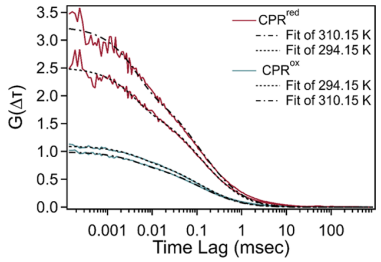

Figure 1. FCS curves and the analysis for Alexa 680-labeled CPR^{red} (upper) and CPR^{ox} (lower) as a function of temperature at 21 and 37 °C. Data collected in the solution above the ER membrane. The data was fit to a triplet model (eq 1). Individual fits for the full temperature range are found in the Supporting Information.

where T_{eq} is the equilibrium triplet fraction, τ is the lag time, τ_D is the average residence time of the protein in the detection volume, τ_T is the triplet relaxation time (different from the triplet lifetime), s is the beam waist, u is the radius along the optical axis, V_{eff} is the effective probe volume (measured to be 1.18 fL), N_A is Avogadro's number, and $\langle C \rangle$ is the concentration of labeled proteins in solution.

Figure 2 summarizes the temperature-dependent concentrations of CPR^{ox} and CPR^{red} in solution as determined from

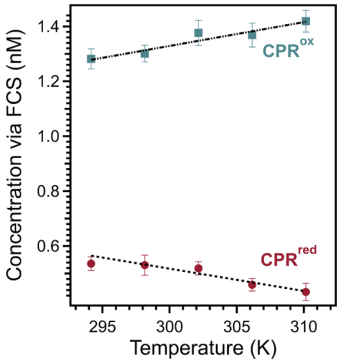

Figure 2. Concentration of Alexa 680-labeled CPR^{ox} (blue squares) and CPR^{red} (red circles) in solution above the ER membrane as a function of temperature. The concentrations were determined from the FCS analysis using eqs 1 and 2. The lines drawn through the data are linear trend lines.

eq 1. In these experiments, a 25 μL droplet of a 2.5 nM solution of either CPR^{ox} or CPR^{red} was allowed to equilibrate with the ER membrane and the CPR concentration in the droplet was then measured using FCS. Figures 1 and 2 show that the solution concentration of CPR^{ox} is greater than that of CPR^{red} at all temperatures. This is consistent with our earlier observations that demonstrated that CPR^{red} is predominately an integral membrane protein, and CPR^{ox} shows some characteristics of being a peripheral membrane protein.[14] The current study clearly demonstrates that the partitioning of CPR from the solution phase to the membrane phase is temperature-dependent. We also observed that the solution phase concentration increases with temperature for CPR^{ox} and decreases with temperature for CPR^{red}. This indicates fundamentally different processes that lead to CPR-membrane interactions that depend on whether it is oxidized or reduced.

3.2. Partitioning Coefficients. In a parallel experiment, the number of CPR^{ox} and CPR^{red} molecules was counted within a 1600 μm^2 area of the ER membrane as a function of temperature using the single-molecule tracking microscope described in Section 2.7. While it is known that FCS experiments are accurate in determining concentrations in very dilute solutions, it is also known that single-molecule fluorescence imaging can severely undercount the number fluorescent molecules in the field of view.[27] The undercounting is due to the blinking and bleaching seen in single-molecule fluorescence trajectories. Depending on the fluorescent probe, the blinking and bleaching rates can also be affected by the temperature and redox environment. In FCS, the fluctuations due to blinking and bleaching can be easily accounted for within the fluorescence correlation fitting function (made possible by the high temporal resolution in modern correlators; 32 ps time bins in our instrument). On the other hand, the single-molecule fluorescence trajectories measured in a wide-field TIRF experiment have a much slower time resolution (50 ms per frame in the present study). Since there is a large buildup of molecules in a dark state in this time frame (triplet or photochemical), undercounting is inevitable. This along with temperature affecting the blinking and bleaching rates leads to unreliable thermodynamic values when the comparison is between multiple phases and temperatures. In this work, we avoided the molecular counting problem seen in single-molecule fluorescent trajectories by only using the FCS data for the thermodynamic analysis. Here, the single-molecule tracking was used to qualitatively verify that the trend in the membrane coincided with the FCS experiments. Figure 3

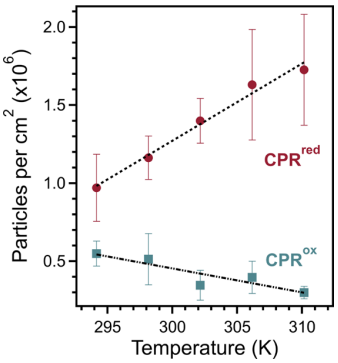

Figure 3. Surface density of freely diffusing Alexa 680-labeled CPR^{ox} (blue squares) and CPR^{red} (red circles) in the ER membrane as a function of temperature. The lines drawn through the data are linear trend lines for the corresponding data. The histograms used for each point can be found in Figure S1, and the means used are in Table S2.

depicts the results of these single-molecule imaging experiments in which the number of CPR^{ox} molecules in the ER membrane decreases with temperature, and the number of CPR^{red} molecules increases with temperature. These trends are consistent with the solution phase studies, showing that the concentration in solution decreases as the number of particles in the membrane increases and *vice versa*. The FCS data along with the trends seen in the single-molecule fluorescence imaging experiments lead to the following equilibrium equation for the partitioning of CPR from the liquid phase into the ER and its corresponding partitioning coefficient (equilibrium constant)[28]

https://doi.org/10.1021/acs.jpcb.1c09358
J. Phys. Chem. B 2022, 126, 1691−1699

$$\mathrm{CPR}^{\mathrm{solution}} \rightleftharpoons \mathrm{CPR}^{\mathrm{membrane}} \tag{2}$$

$$K_{\mathrm{p}} = \frac{[\mathrm{CPR}]^{\mathrm{membrane}}}{[\mathrm{CPR}]^{\mathrm{solution}}} \tag{3}$$

where $[\mathrm{CPR}]^{\mathrm{membrane}}$ is the concentration of CPR in the ER and $[\mathrm{CPR}]^{\mathrm{solution}}$ is the concentration of CPR in the droplet above the ER. The concentration of CPR in the membrane was determined from eq 4 below

$$[\mathrm{CPR}]^{\mathrm{solution}} = \frac{\mathrm{CPR}_{\mathrm{total}}^{\mathrm{moles}} - \mathrm{CPR}_{\mathrm{sol}}^{\mathrm{moles}}}{V_{\mathrm{mem}}} \tag{4}$$

where $\mathrm{CPR}_{\mathrm{total}}^{\mathrm{moles}}$ is the total number of moles of CPR in the droplet before equilibrium, which was determined from a UV−vis experiment of the stock solution before placing the diluted sample on the ER membrane, $\mathrm{CPR}_{\mathrm{sol}}^{\mathrm{moles}}$ is the number of moles in the droplet once equilibrium is reached with the ER membrane being obtained from FCS data (see Figure 2), and V_{mem} is the total volume of the ER membrane. V_{mem} was estimated from the thickness of the membrane, the height that CPR protrudes from the membrane, and the total area of the membrane. The thickness was estimated previously by taking the thickness of the ER membrane to be the same as its major component (POPC, which is 30 Å) and the height of CPR protruding from the ER membrane (which is 44 Å as measured by neutron reflectivity).[11,12,17] The area of the membrane (0.283 cm^2) was assumed to be the same as the paraffin gasket used to contain the ER membrane on the glass coverslip. The initial concentration of CPR in the droplet was 2.5 nM, and the concentration of CPR in the droplet after equilibrium is plotted in Figure 2. Using these data, the partition coefficients were calculated and are summarized in Table S1. Taking the standard state to be 25 °C and 1 M, the standard state partitioning coefficients are $K_{\mathrm{P}}^{\mathrm{ox}}(25°\mathrm{C}) = 1.10 \times 10^5$ for the oxidized form and $K_{\mathrm{P}}^{\mathrm{red}}(25°\mathrm{C}) = 4.44 \times 10^5$ for the reduced form.

3.3. Standard State Gibbs Free Energies, Enthalpies, and Entropies. The partitioning coefficients (K_{p}, eq 3) were measured between 21 and 37 °C as described above in 4 °C increments. Assuming that the enthalpy and entropy do not change much in this temperature range, the van't Hoff equation can be written as (eq 5)

$$\ln(K_{\mathrm{p}}) = -\frac{\Delta H_{\mathrm{P}}^{\circ}}{RT} + \frac{\Delta S_{\mathrm{P}}^{\circ}}{R} \tag{5}$$

where $\Delta H_{\mathrm{P}}^{\circ}$ and $\Delta S_{\mathrm{P}}^{\circ}$ are the standard state enthalpies and entropies for CPR interacting with the ER, respectively. The slopes of the curves in Figure 4 give $\Delta H_{\mathrm{P,\,ox}}^{\circ} = -11$ kJ mol^{-1} and $\Delta H_{\mathrm{P,\,red}}^{\circ} = 15$ kJ mol^{-1}. These results show that $\mathrm{CPR}^{\mathrm{ox}}$ insertion into the ER membrane is an exothermic process, and $\mathrm{CPR}^{\mathrm{red}}$ is an endothermic process. The standard state entropies are determined from the intercepts of the curves in Figure 5, which are $\Delta S_{\mathrm{P,\,ox}}^{\circ} = 61$ J mol^{-1} K^{-1} and $\Delta S_{\mathrm{P,\,red}}^{\circ} = 160$ J mol^{-1} K^{-1}. From eq 6

$$\Delta G_{\mathrm{P}}^{\circ} = \Delta H_{\mathrm{P}}^{\circ} - T\Delta S_{\mathrm{P}}^{\circ} \tag{6}$$

$\Delta G_{\mathrm{P,\,ox}}^{\circ} = -28$ kJ mol^{-1} and $\Delta G_{\mathrm{P,\,red}}^{\circ} = -32$ kJ mol^{-1}. Alternatively, it is known that enthalpy changes slowly with temperature and it is a good approximation to assume that it is temperature-independent over a small temperature range (not always the case with entropy). This allows us to pick a standard state temperature (25 °C in this study) and measure the partitioning coefficient from the experiment (see Section 3.2) without making any assumptions about entropy. $\Delta G_{\mathrm{P,\,red}}^{\circ}(25°\mathrm{C})$ can then be determined from

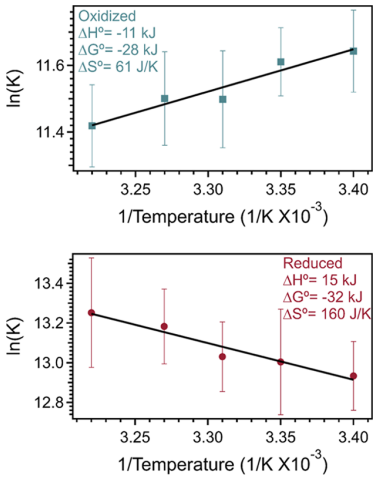

Figure 4. Arrhenius plots of Alexa 680-labeled $\mathrm{CPR}^{\mathrm{ox}}$ (upper curve) and $\mathrm{CPR}^{\mathrm{red}}$ (lower curve). The partition coefficients K_{p} are given in eq 3, and the data (Table S3) was fit to the Arrhenius equation (black lines through the data). The standard change in Gibbs free energies was calculated from eq 7 at 25 °C, the standard enthalpies were determined from the slope of the Arrhenius plot (eq 5), and the change in standard entropy was determined from equations ΔG°, ΔH°, and eq 6.

$$\Delta G_{\mathrm{P}}^{\circ}(25°\mathrm{C}) = -RT\ln(K_{\mathrm{P}}^{\circ}(25°\mathrm{C})) \tag{7}$$

$\Delta H_{\mathrm{P}}^{\circ}(25°\mathrm{C})$ is determined from

$$\ln\left(\frac{K_{\mathrm{p}}(T)}{K_{\mathrm{P}}^{\circ}(25°\mathrm{C})}\right) = -\frac{\Delta H_{\mathrm{P}}^{\circ}}{R}\left(\frac{1}{T} - \frac{1}{298.15\mathrm{K}}\right) \tag{8}$$

and $\Delta S_{\mathrm{P}}^{\circ}(25°\mathrm{C})$ is determined from eq 6. Carrying this analysis forward gives $\Delta G_{\mathrm{P,\,ox}}^{\circ}(25°\mathrm{C}) = -28$ kJ mol^{-1}, $\Delta S_{\mathrm{P,\,ox}}^{\circ}(25°\mathrm{C}) = 61$ J mol^{-1} K^{-1}, $\Delta G_{\mathrm{P,\,red}}^{\circ}(25°\mathrm{C}) = -32.2$ kJ mol^{-1}, and $\Delta S_{\mathrm{P,\,red}}^{\circ}(25°\mathrm{C}) = 161$ J mol^{-1} K^{-1}. These values are in close agreement with eq 5 and demonstrate that entropy changes little over the experimental temperature range. A figure of the analysis using eq 8 is included in the Supporting Information (Figure S3), and a table of thermodynamic values with errors is included in Table S4.

4. DISCUSSION

The thermodynamic driving forces for CPR partitioning into an ER membrane are drastically dependent on whether CPR is oxidized or reduced. Both redox states of CPR have a chemical potential that strongly favors partitioning into the ER membrane at 25 °C, but the process is more favored for $\mathrm{CPR}^{\mathrm{red}}$ than $\mathrm{CPR}^{\mathrm{ox}}$. Interestingly, even though $K_{\mathrm{P}}^{\mathrm{red}} > K_{\mathrm{P}}^{\mathrm{ox}}$ for all conditions measured in this study, the process is exothermic for $\mathrm{CPR}^{\mathrm{ox}}$ and endothermic for $\mathrm{CPR}^{\mathrm{red}}$. Therefore, as temperature rises, the membrane partitioning of $\mathrm{CPR}^{\mathrm{ox}}$ decreases and $\mathrm{CPR}^{\mathrm{red}}$ increases. In addition, the $\Delta S_{\mathrm{P}}^{\circ}$ is positive for both $\mathrm{CPR}^{\mathrm{ox}}$ and $\mathrm{CPR}^{\mathrm{red}}$ but is 2.6 times larger for $\mathrm{CPR}^{\mathrm{red}}$ than $\mathrm{CPR}^{\mathrm{ox}}$. Moreover, our earlier studies have shown that $\mathrm{CPR}^{\mathrm{red}}$ diffuses more slowly than $\mathrm{CPR}^{\mathrm{ox}}$ in an ER membrane (1.5 $\mu\mathrm{m}^2$/s compared to 2.5 $\mu\mathrm{m}^2$/s) and that $\mathrm{CPR}^{\mathrm{ox}}$ shows some characteristics of a peripheral membrane protein

https://doi.org/10.1021/acs.jpcb.1c09358
J. Phys. Chem. B 2022, 126, 1691−1699

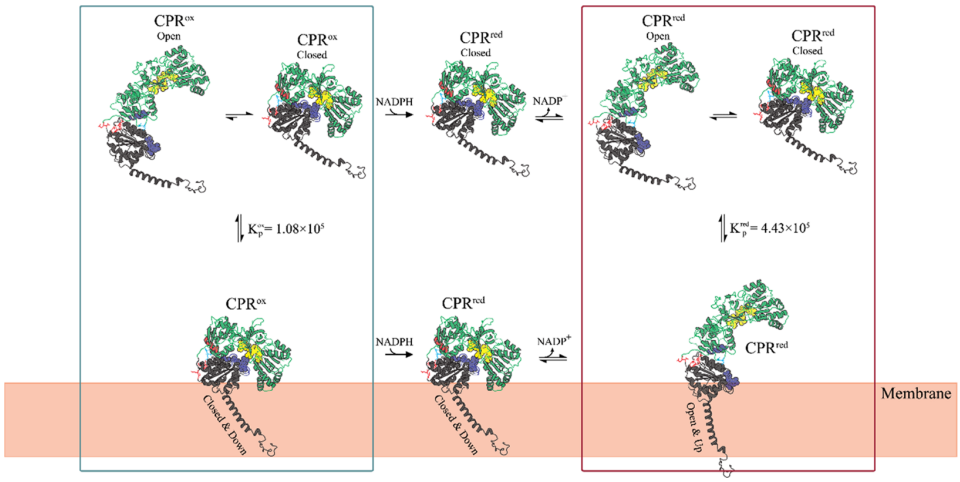

Figure 5. Sketch depicting the redox state-dependent interaction of CPR with the ER. The MBD is depicted in dark gray as an alpha helix, while FMN and FAD are the blue and yellow prosthetic groups that are separated by a hinge domain, respectively, allowing for a confirmational change between open and closed states. Starting from the left, CPR is in the oxidized state and in solution from which it is able to insert into the lipid bilayer in down orientation. Once in the bilayer, NADPH binds to the protein transferring its electrons, reducing CPR. As $NADP^+$ unbinds, it leaves CPR^{red} in an open conformation and an up orientation relative to the membrane surface. Finally, in solution, the equilibrium conformation of CPR^{red} is a near 50:50 equilibrium between open and closed conformations. The process of reduction in solution is also shown following the same steps as the lipid population. The blue and red boxes represent the parts of the model measured in this study.

while CPR^{red} shows none.[14] All together, these results suggested that the membrane binding domain (MBD) of CPR^{red} is more deeply embedded into the ER membrane, which decreases its diffusion coefficient and results in a greater partitioning over CPR^{ox}. The results of this study are consistent with those earlier conclusions. This study presents evidence that the drastically different changes in enthalpy (endothermic vs exothermic) and large differences in entropy are probably more due to the overall conformational change of this multidomain protein (FAD/NADPH, FMN, Hinge domains) and how they interact with the surface of the ER and then insertion of the MBD, which is similar for both redox states.

It is well known that CPR has two conformational states: open and closed.[6−9,12] The open state is the conformation in which the FAD and FMN domains are furthest apart, and the closed conformation is when the two domains are closest to one another, allowing inter-flavin electron transfer. Using solution phase NMR and SAXS (small-angle X-ray scattering), it was demonstrated that CPR^{ox} is predominately in its closed state with only a small percent existing in the open state (5−7.5% according to Vincent et al. and 15% according to Huang et al.).[9,12] This was later confirmed by Jenner et al. using ionization ion mobility spectrometry (IMS).[29] Roberts et al. also concluded that the conformational distribution of CPR^{red} is pushed more toward the open conformation in solution but still has a significant, if smaller, population in the closed state (they did not estimate the percent distribution of the populations for CPR^{red}).[12] These results are consistent with a recent cryo-EM study conducted by Su et al. that demonstrated the conformational flexibility between open and closed states of the CPR domain in dimeric cytochrome P450 CYP102A1.[30] A simplified electron transfer mechanism is as follows: (i) CPR^{ox} starts in its mostly closed conformation and is ready to accept a NADPH ligand, (ii) NADPH then binds to CPR^{ox} where it undergoes a two-electron reduction through a hydride ion transfer to FAD and subsequent inter-flavin electron transfer, and (iii) $NADP^+$ is then released, leaving CPR^{red} in an equilibrium that favors the open position.[11,12,31] Moreover, a recent computational study carried out by Sellner et al.[15] using molecular dynamics simulations to map out the conformational landscape of CPR in a membrane describes four important observations: (i) CPR^{ox} in its closed conformation favors a position in which the FAD and FMN domains are orientated face down into the membrane, resulting in significant protein−lipid interactions (closed-down position); (ii) upon reduction, CPR^{red} favors an open conformation and flips to a position in which the FAD and FMN domains face away from the surface of the membrane (open-up position), breaking the superficial membrane contacts found in the closed-down position; (iii) in the closed-down position, CPR has two energetically favorable closely related conformational states, while (iv) in the open-up position, there are no discernable minima and CPR^{red} occupies a rather large conformational landscape (i.e., it is highly flexible).[15] Though not mentioned in Sellner et al.'s paper, we have interpreted their results to mean that, while embedded in the membrane, the closed-down position is in a relatively low entropy state (not flexible) and has favorable protein−lipid interactions in comparison to the open-up position that is more flexible (more entropic) but lacks favorable protein−lipid interactions. It is also true that trapped solvent molecules in the interface between globular domains in a close conformation will be liberated in the open conformation, and the lipid molecules in the vicinity of the vertically aligned MBD of CPR^{red} should be less structured than those near the MBD of CPR^{ox} adding to the higher entropy in the open-up position. Sellner et al. also demonstrated that, when in the open-up position, the MBD has a more vertical orientation in the membrane (deeper penetration) than it has in the closed-down position. Finally, the equilibrium between the open and closed conformation and their orientation relative to the membrane (up and down) still exists but CPR^{ox} favors the closed-down state and CPR^{red}

https://doi.org/10.1021/acs.jpcb.1c09358
J. Phys. Chem. B 2022, 126, 1691−1699

favors the open-up state. A phenomenological model that only includes the dominant membrane states and equilibrium solution states is summarized in Figure 5. A solution phase reduction pathway is also included in Figure 5.

In this study, the samples were equilibrated in the oxidized and reduced states in the presence of an ER membrane. The thermodynamic driving forces of partitioning were then measured. These processes are indicated by the red and blue squares in Figure 5, but the measured partitioning is more correctly described as between all conformational states between solution and membrane phases for each redox state. Besides the reorientation of the MBD, the conformational states (open vs closed) and the orientation relative to the membrane (up vs down) have profound effects on the thermodynamic driving forces keeping CPR in the membrane as indicated above. CPR^{ox} is >92% closed in solution and will probably remain, so when entering the membrane, the significant contacts between the globular domains of CPR^{ox} with the membrane can lead to a favorable protein−lipid enthalpic interaction (exothermic) and a positive entropy change as the MBD embeds into the membrane and as water associated with the bilayer is displaced by CPR^{ox}. In total, this should lead to a favorable free energy change (negative) that drives the partitioning of CPR^{ox} into the ER.

CPR^{red} is hypothesized to primarily be in the in the open-up position in the membrane, and CPR^{red} in solution has a significant population in both open and closed states. While the driving forces responsible for the membrane orientation are up for debate, the extra negative charge on $FMNH_2$ or FMNH· will certainly cause some electrostatic repulsion with the negatively charged ER membrane surface. With this in mind, as CPR^{red} partitions into the membrane, the electrostatic repulsion and lack of significant contacts between the globular domains and membrane cause an endothermic change in enthalpy. As discussed, the open-up position has increased entropy in comparison to the closed conformation because of flexibility and no well-defined minimum in its potential energy surface (see above). If the equilibrium distribution between open and closed states shifts more toward the open configuration when entering the membrane, then the added entropy gained from being predominantly in the open position may contribute to the larger entropy change observed in CPR^{red} partitioning. Regardless of the explanation, our experiments clearly show that the entropic changes significantly outweigh the enthalpic changes, leading to a highly favorable free energy driving force for membrane partitioning for CPR^{red}.

5. CONCLUSIONS

Cytochrome P450 reductase is an important di-flavin oxidoreductase that is a redox partner for nearly all P450 enzymes. Presented in this work are the measured free energies, enthalpies, and entropies of human CPR insertion into ER membranes as a function of the redox state and temperature. This was accomplished using FCS and single-protein tracking to directly measure the partitioning coefficients (and therefore free energies), while enthalpies and entropies were determined using a van't Hoff analysis. These measurements have shown that (i) the thermodynamic driving force for CPR^{red} insertion into an ER membrane is due to a large change in entropy that outweighs an endothermic enthalpy change, and (ii) the thermodynamic driving forces for CPR^{ox} insertion are due to a negative enthalpy change and a smaller positive entropy change. A standard state of 25 °C, pH 7.4, and physiological ionic strength were chosen, and the standard state Gibbs free energy, enthalpy, and entropy changes for CPR insertion were determined for each redox state ($\Delta G^{o}_{P,ox}(25°C) = -28$ kJ mol^{-1}, $\Delta H^{o}_{P,ox} = -11$ kJ mol^{-1}, and $\Delta S^{o}_{P,ox}(25°C) = 61$ J mol^{-1} K^{-1}; $\Delta G^{o}_{P,red}(25°C) = -32.2$ kJ mol^{-1}, $\Delta H^{o}_{P,red} = 15$ kJ mol^{-1}, and $\Delta S^{o}_{P,red}(25°C) = 161$ J mol^{-1} K^{-1}, respectively). These results are consistent with a model in which CPR^{ox} is predominately in its closed conformation in solution and predominately in the closed-down position in the ER membrane and the CPR^{red} equilibrium shifted to the closed conformation in solution and an open-up position in the ER membrane.

■ ASSOCIATED CONTENT

Supporting Information

The Supporting Information is available free of charge at https://pubs.acs.org/doi/10.1021/acs.jpcb.1c09358.

All histograms from the single-protein tracking experiments along with fits, all raw FCS data and corresponding fits, figure summarizing the temperature dependence of the K_Ps, which is also tabulated in Table S1, an Arrhenius plot according to eq 8, and table summarizing Gibbs free energies, enthalpies, and entropies (PDF)

(PDF)

■ AUTHOR INFORMATION

Corresponding Author

J. A. Brozik − *Department of Chemistry, Washington State University, Pullman, Washington 99163-4630, United States; Materials Science & Engineering Program, Washington State University, Pullman, Washington 99163-2711, United States;* orcid.org/0000-0003-2097-5051; Email: brozik@wsu.edu

Authors

Michael J. Martinez − *Department of Chemistry, Washington State University, Pullman, Washington 99163-4630, United States*

Jessica D. Carder − *Department of Chemistry, Washington State University, Pullman, Washington 99163-4630, United States*

Evan L. Taylor − *Materials Science & Engineering Program, Washington State University, Pullman, Washington 99163-2711, United States;* orcid.org/0000-0002-6460-1871

Eric P. Jacobo − *Department of Chemistry, Washington State University, Pullman, Washington 99163-4630, United States*

ChulHee Kang − *Department of Chemistry, Washington State University, Pullman, Washington 99163-4630, United States*

Complete contact information is available at: https://pubs.acs.org/10.1021/acs.jpcb.1c09358

Author Contributions

The manuscript was written through contributions of all authors. All authors have given approval to the final version of the manuscript.

Notes

The authors declare no competing financial interest.

https://doi.org/10.1021/acs.jpcb.1c09358
J. Phys. Chem. B 2022, 126, 1691−1699

■ ACKNOWLEDGMENTS

The authors acknowledge the National Science Foundation MCB-2043248 (to C.K. and J.A.B.).

■ ABBREVIATIONS

CPR cytochrome P450 reductase; FCS fluorescence correlation spectroscopy; NADPH nicotinamide adenine dinucleotide phosphate; HEPES 4-(2-hydroxyethyl)-1-piperazineethanesulfonic acid; DTT 1,4-dithiothreitol; Tris buffer *tris*(hydroxymethyl)-aminomethane; PEG polyethylene glycol; SUV small unilamellar vesicle; DLPC 1,2-dilauroyl-*sn*-glycero-3-phosphocholine; DOPC 1,2-dioleoyl-*sn*-glycero-3-phosphocholine; POPE 1-palmitoyl-2-oleoyl-*sn*-glycero-3-phosphoethanolamine; DLPS 1,2-dilauroyl-*sn*-glycero-3-phospho-L-serine; PEG−PE 1,2-dioleoyl-*sn*-glycero-3-phosphoethanolamine-*N*-[methoxy(polyethylene glycol)-2000]; LMV large multilamellar vesicle; ER buffer 100 mM HEPES, 5 mM $CaCl_2$, and 140 mM NaCl at pH 7.4; nanopure water water that was purified by a Barnsted Nanopure 18 MΩ organic free water purifier; TIRF total internal reflection fluorescence microscopy; MBD membrane binding domain; FMN flavin mononucleotide; FAD flavin adenine dinucleotide; ER endoplasmic reticulum; CPR^{red} reduced cytochrome P450 reductase; CPR^{ox} oxidized cytochrome P450 reductase

■ REFERENCES

(1) Pandey, A. V.; Fluck, C. E. NADPH P450 oxidoreductase: structure, function, and pathology of diseases. *Pharmacol. Ther.* **2013**, *138*, 229−254.
(2) Montellano, P. R. O. D., *Cytochrome P450: structure, mechanism, and biochemistry*. 3 ed.; Springer, 2005.
(3) Denisov, I. G.; Makris, T. M.; Sligar, S. G.; Schlichting, I. Sligar, and Ilme Schlichting, Structure and Chemistry of Cytochrome P450. *Chem. Rev.* **2005**, *105*, 2253−2278.
(4) Wang, M.; Roberts, D. L.; Paschke, R.; Shea, T. M.; Masters, B. S. S.; Kim, J.-J. P. Three-dimensional structure of NADPH−cytochrome P450 reductase: Prototype for FMN- and FAD-containing enzymes. *Proc. Natl. Acad. Sci.* **1997**, *94*, 8411−8416.
(5) Zhao, Q.; Modi, S.; Smith, G.; Paine, M.; McDonagh, P. D.; Wolf, C. R.; Tew, D.; Lian, L.-Y.; Roberts, G. C. K.; Driessen, H. P. C. Crystal structure of the FMN-binding domain of human cytochrome P450 reductase at 1. 93 Å resolution. *Protein Sci.* **1999**, *8*, 298−306.
(6) Murataliev, M. B.; Feyereisen, R.; Walker, F. A. Electron transfer by diflavin reductases. *Biochim. Biophys. Acta, Proteins Proteomics* **2004**, *1698*, 1−26.
(7) Ellis, J.; Gutierrez, A.; Barsukov, I. L.; Huang, W. C.; Grossmann, J. G.; Roberts, G. C. Domain motion in cytochrome P450 reductase: conformational equilibria revealed by NMR and small-angle x-ray scattering. *J. Biol. Chem.* **2009**, *284*, 36628−36637.
(8) Gutierrez, A.; Grunau, A.; Paine, M.; Munro, A. W.; Wolf, C. R.; Roberts, G. C. K.; Scrutton, N. S. Electron transfer in human cytochrome P450 reductase. *Biochem. Soc. Trans.* **2003**, *31*, 497−501.
(9) Vincent, B.; Morellet, N.; Fatemi, F.; Aigrain, L.; Truan, G.; Guittet, E.; Lescop, E. The Closed and Compact Domain Organization of the 70-kDa Human Cytochrome P450 Reductase in Its Oxidized State As Revealed by NMR. *J. Mol. Biol.* **2012**, *420*, 296−309.
(10) Das, A.; Sligar, S. G. Modulation of the cytochrome P450 reductase redox potential by the phospholipid bilayer. *Biochemistry* **2009**, *48*, 12104−12112.
(11) Wadsäter, M.; Laursen, T.; Singha, A.; Hatzakis, N. S.; Stamou, D.; Barker, R.; Mortensen, K.; Feidenhans'l, R.; Møller, B. L.; Cárdenas, M. Monitoring Shifts in the Conformation Equilibrium of the Membrane Protein Cytochrome P450 Reductase (POR) in Nanodiscs*. *J. Biol. Chem.* **2012**, *287*, 34596−34603.
(12) Huang, W.-C.; Ellis, J.; Moody, P. C. E.; Raven, E. L.; Roberts, G. C. K. Redox-linked domain movements in the catalytic cycle of cytochrome p450 reductase. *Structure* **2013**, *21*, 1581−1589.
(13) Estrada, D. F.; Laurence, J. S.; Scott, E. E. Cytochrome P450 17A1 Interactions with the FMN Domain of Its Reductase as Characterized by NMR*. *J. Biol. Chem.* **2016**, *291*, 3990−4003.
(14) Barnaba, C.; Martinez, M. J.; Taylor, E.; Barden, A. O.; Brozik, J. A. Single Protein Tracking Reveals that NADPH Mediates the Insertion of Cytochrome P450-Reductase into a Biomimetic of the Endoplasmic Reticulum. *J. Am. Chem. Soc.* **2017**, *139*, 5420−5430.
(15) Sellner, M.; Fischer, A.; Don, C. G.; Smiesko, M. Conformational Landscape of Cytochrome P450 Reductase Interactions. *Int. J. Mol. Sci.* **2021**, *22*, 1023.
(16) Rock, D.; Rock, D.; Jones, J. P. Inexpensive purification of P450 reductase and other proteins using 2′, 5′-adenosine diphosphate agarose affinity columns. *Protein Expression Purif.* **2001**, *22*, 82−83.
(17) Barnaba, C.; Taylor, E.; Brozik, J. A. Dissociation Constants of Cytochrome P450 2C9/Cytochrome P450 Reductase Complexes in a Lipid Bilayer Membrane Depend on NADPH: A Single-Protein Tracking Study. *J. Am. Chem. Soc.* **2017**, *139*, 17923−17934.
(18) Kumud, R. P.; Jeffrey, P. J.; James, A. B. A guide to tracking single transmembrane proteins in supported lipid bilayers. In *Lipid-Proteins Interactions*, Humana Press: 2013; Vol. *974*, pp. 233−252, DOI: 10.1007/978-1-62703-275-9_11.
(19) Barnaba, C.; Humphreys, S.; Barden, A.; Jones, J.; Brozik, J. Substrate Dependent Native Luminescence From Cytochromes P450 3A4, 2C9, and P450cam. *J. Phys. Chem. B* **2016**, *120*, 3038−3047.
(20) Yildiz, A.; Forkey, J. N.; McKinney, S. A.; Ha, T.; Goldman, Y. E.; Selvin, P. R. Myosin V Walks Hand-Over-Hand: Single Fluorophore Imaging with 1. 5-nm Localization. *Science* **2003**, *300*, 2061−2065.
(21) Waskell, L.; Kim, J.-J. P., Electron Transfer Partners of Cytochrome P450. In *Cytochrome P450: Structure, Mechanism, and Biochemistry*, Ortiz de Montellano, P. R., Ed. Springer International Publishing: Cham, 2015; pp. 33−68.
(22) Iyanagi, T.; Mason, H. S. Properties of hepatic reduced nicotinamide adenine dinucleotide phosphate-cytochrome c reductase. *Biochemistry* **1973**, *12*, 2297−2308.
(23) Iyanagi, T.; Makino, R.; Anan, F. K. Studies on the microsomal mixed-function oxidase system: mechanism of action of hepatic NADPH-cytochrome P-450 reductase. *Biochemistry* **1981**, *20*, 1722−1730.
(24) Rüttinger, S.; Buschmann, V.; Krämer, B.; Erdmann, R.; Macdonald, R.; Koberling, F., *Determination of the confocal volume for quantitative fluorescence correlation spectroscopy*. SPIE: 2007; Vol. *6630*.
(25) Crocker, J. C.; Grier, D. G. Methods of digital video microscopy for colloidal studies. *J. Colloid Interface Sci.* **1996**, *179*, 298−310.
(26) Schwille, P.; Haustein, E. In *Fluorescence Correlation Spectroscopy An Introduction to its Concepts and Applications*, 2002.
(27) Rollins, G. C.; Shin, J. Y.; Bustamante, C.; Pressé, S. Stochastic approach to the molecular counting problem in superresolution microscopy. *Proc. Natl. Acad. Sci.* **2015**, *112*, E110.
(28) Davis, R. W.; Patrick, E. L.; Meyer, L. A.; Ortiz, T. P.; Marshall, J. A.; Keller, D. J.; Brozik, S. M.; Brozik, J. A. Thermodynamic Properties of Single Ion Channel Formation: Gramicidin. *J. Phys. Chem. B* **2004**, *108*, 15364−15369.
(29) Jenner, M.; Ellis, J.; Huang, W. C.; Lloyd Raven, E.; Roberts, G. C.; Oldham, N. J. Detection of a protein conformational equilibrium by electrospray ionisation-ion mobility-mass spectrometry. *Angew. Chem., Int. Ed.* **2011**, *50*, 8291−8294.
(30) Su, M.; Chakraborty, S.; Osawa, Y.; Zhang, H. Cryo-EM reveals the architecture of the dimeric cytochrome P450 CYP102A1 enzyme and conformational changes required for redox partner recognition. *J. Biol. Chem.* **2020**, *295*, 1637−1645.
(31) Huang, R.; Yamamoto, K.; Zhang, M.; Popovych, N.; Hung, I.; Im, S.-C.; Gan, Z.; Waskell, L.; Ramamoorthy, A. Probing the Transmembrane Structure and Dynamics of Microsomal NADPH-

cytochrome P450 oxidoreductase by Solid-State NMR. *Biophys. J.* **2014**, *106*, 2126−2133.

https://doi.org/10.1021/acs.jpcb.1c09358
J. Phys. Chem. B 2022, 126, 1691−1699